

CHEMISTRY

A European Journal

A Journal of



Accepted Article

Title: Tailored Design of Bicontinuous Gyroid Mesoporous Carbon and Nitrogen-Doped Carbon from Poly(ethylene oxide-*b*-caprolactone) Diblock Copolymers

Authors: Shiao-Wei Kuo, Wei-Cheng Chu, Bishnu Prasad Bastakoti, Yusuf Valentino Kaneti, Jheng-Guang Li, Yusuke Yamauchi, Hatem R. Alamri, and Zeid A. Allothman

This manuscript has been accepted after peer review and appears as an Accepted Article online prior to editing, proofing, and formal publication of the final Version of Record (VoR). This work is currently citable by using the Digital Object Identifier (DOI) given below. The VoR will be published online in Early View as soon as possible and may be different to this Accepted Article as a result of editing. Readers should obtain the VoR from the journal website shown below when it is published to ensure accuracy of information. The authors are responsible for the content of this Accepted Article.

To be cited as: *Chem. Eur. J.* 10.1002/chem.201702360

Link to VoR: <http://dx.doi.org/10.1002/chem.201702360>

Supported by
ACES

WILEY-VCH

Tailored Design of Bicontinuous Gyroid Mesoporous Carbon and Nitrogen-Doped Carbon from Poly(ethylene oxide-*b*-caprolactone) Diblock Copolymers

Wei-Cheng Chu,¹ Bishnu Prasad Bastakoti,² Yusuf Valentino Kaneti,² Jheng-Guang Li,^{1,3} Hatem R. Alamri,⁴ Zeid A. Allothman,⁵ Yusuke Yamauchi,^{2,5,6*} and Shiao-Wei Kuo^{1,7*}

1 *Materials and Optoelectronic Science, National Sun Yat-Sen University, Center for Nanoscience and Nanotechnology, Kaohsiung, 804, Taiwan*

2 *World Premier International (WPI) Research Center for Materials Nanoarchitectonics (MANA), National Institute for Materials Science (NIMS), 1-1 Namiki, Tsukuba, Ibaraki 305-0044 (Japan)*

3 *R&D Department, Asia Carbons & Technology Inc., Taoyuan, Taiwan*

4 *Physics Department, Jamoum University College, Umm Al-Qura University, Makkah, 21955, Saudi Arabia*

5 *Advanced Materials Research Chair, Chemistry Department, College of Science, King Saud University, Riyadh 11451, Saudi Arabia*

6 *Australian Institute for Innovative Materials (AIIM), University of Wollongong, Squires Way, North Wollongong, NSW 2500, Australia*

7 *Department of Medicinal and Applied Chemistry, Kaohsiung Medical University, Kaohsiung, Taiwan*

E-mails: kuosw@faculty.nsysu.edu.tw; yusuke@uow.edu.au

Abstract: Highly ordered mesoporous resol-type phenolic resin and the corresponding mesoporous carbon materials have been synthesized by using PEO-*b*-PCL diblock copolymer as a soft-template. The self-assembled mesoporous phenolic resin was found to form only at a specific resol concentration range of 40-70 wt% through the intriguing balance of hydrogen bonding interactions in the resol/PEO-*b*-PCL mixtures. Furthermore, the morphological transitions of the mesostructures from disordered to gyroid to cylindrical and finally to disordered micelle structure were observed with the increasing resol concentrations. By calcination under nitrogen atmosphere at 800 °C, the bicontinuous mesostructured gyroid phenolic resin can be converted to mesoporous carbon with large pore size without the collapse of the original mesostructure. Furthermore, the post-treatment of the mesoporous gyroid phenolic resin with melamine gave rise to N-doped mesoporous carbon with unique electronic properties for realizing a high CO₂ adsorption (6.72 mmol·g⁻¹ at 0 °C).

Introduction

Amphiphilic molecules, such as surfactants and block copolymers, have been extensively used as soft-templates for the synthesis of ordered mesoporous materials.^[1-3] The discovery of ordered mesoporous carbon materials has attracted a great deal of attention because of their unique physical and chemical properties, which can surmount the shortcomings of disordered carbon materials (*e.g.*, activated carbon) in various applications such as catalysis, sorption, separation, drug delivery, and energy storage materials.^[4-7] So far, hard- and soft-templating approaches have been successfully employed for the preparation of mesoporous carbon materials with well-defined pore structures and narrow pore size distributions. A hard-templating approach typically uses pre-synthesized templates as molds for the replication of nanoporous/mesoporous carbons and does not involve any significant chemical interactions with the carbon precursors.^[8] In this case, the morphology of the resulting carbon materials is pre-determined by the templates which have well-defined nanostructures. In contrast, soft-templating approaches encompass organic species and block copolymers through the self-assembly of organic molecules to form carbon nanostructures. In such cases, the obtained pore structures are determined by the synthetic conditions, such as mixing ratios, solvents, and temperatures. This approach differs from the hard-template

synthesis because the molecules or moieties self-assemble in an oriented manner through specific chemical interactions. These interactions between the template and the carbon precursors are key factors which determine the successful synthesis of carbon nanostructures using soft-templating approach.

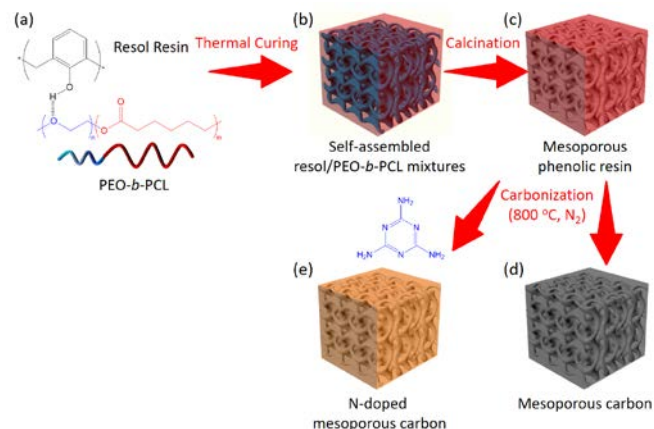
In order to prepare highly ordered mesoporous carbon materials using phenolic resins as the precursors, the following points should be carefully considered: (i) the pre-polymerization in optimal conditions (either in basic (for resol type) or in acidic (for novolac type) medium), (ii) the self-assembly structure through thermal cross-linking by phenolic resin templated by block copolymers, (iii) the block copolymer template removal by calcination, and (iv) the carbonization of phenolic resin under inert atmosphere.^[3] Ikkala *et al.* has reported the fabrication of mesoporous novolac-type phenolic resin templated by poly(styrene-*b*-4-vinyl pyridine) (PS-*b*-P4VP) or poly(isoprene-*b*-2-vinyl pyridine) (PI-*b*-P2VP) diblock copolymers with the curing agent (hexamethylenetetramine, HMTA).^[9-10] Other diblock copolymers, such as poly(ethylene oxide-*b*-styrene) (PEO-*b*-PS)^[11-12], poly(ethylene oxide-*b*-methyl methacrylate) (PEO-*b*-PMMA)^[13], and poly(ethylene oxide-*b*-caprolactone) (PEO-*b*-PCL)^[14-16] are also available for preparation of highly ordered mesoporous phenolic resins and carbons.

Another resol-type of mesoporous phenolic resin could be obtained through the *in-situ* phenolic cross-linking from mixtures containing phenol-derivative, formaldehyde, diblock copolymer, and solvent. Dai *et al.* reported highly ordered mesoporous carbon materials based on the resol-type of phenolic resin by using phloroglucinol, formaldehyde, and F127 triblock copolymer under mild conditions.^[17] Zhao *et al.* proposed the ordered mesoporous carbon by using resol-type of phenolic resin with P123 triblock copolymer.^[18] However, using those commercially available triblock copolymers (Pluronic-type F127 or P123), it is difficult to obtain mesoporous carbon with pore size larger than 10 nm due to the molecular weight limitations. To increase the pore size, highly ordered and large porous mesoporous carbons have been synthesized by using laboratory-synthesized PEO-*b*-PMMA-*b*-PS^[19] and PEO-*b*-PCL-*b*-PLLA^[20] triblock copolymers. Wiesner *et al.* has developed highly ordered mesoporous carbon with a bicontinuous gyroid structure by using PEO-*b*-PS-*b*-PI as a soft template. The obtained pore size was significantly increased up to 39 nm.^[21] However, the synthesis of this triblock copolymer is by using anionic living polymerization is rather difficult.

FULL PAPER

WILEY-VCH

Herein, we report for the first time the synthesis of large-sized mesoporous resol-type phenolic resins and the corresponding mesoporous carbon materials by a soft-templating method using simple PEO-*b*-PCL diblock copolymer as shown in Scheme 1. In addition, nitrogen-doped mesoporous carbons are also synthesized by adding melamine. Previously, the insertion of nitrogen into carbon structures can alter their surface polarity, electrical conductivity, and electron-donor affinity^[22-28], which in turn influence the interactions between the carbon surface and CO₂ molecules. As proof-of-concept, we demonstrate that the obtained N-doped mesoporous materials can be utilized as very effective CO₂ adsorbents.



Scheme 1. A schematic illustration of the preparation of N-doped mesoporous carbon. (a) Mixture of resol and PEO-*b*-PCL, (b) self-assembled resol/PEO-*b*-PCL mixtures through thermal curing, (c) mesoporous phenolic resin through calcination, (d) mesoporous carbon by subsequent carbonization at 800 °C under N₂ atmosphere, and (e) N-doped mesoporous carbon modification by addition of melamine followed by subsequent carbonization at 800 °C under N₂ atmosphere.

Results and Discussion

Self-assembled resol/PEO-*b*-PCL mixtures. In general, the cooling scan of DSC thermograms is a convenient approach for determining the crystallization behavior, since the crystallization or freezing temperature (T_f) is correlated to the self-assembly structures of block copolymers.^[14,29] **Figure 1a** displays the DSC cooling scan of resol/PEO-*b*-PCL mixtures. Clearly, pure PEO-*b*-PCL diblock copolymer shows a T_f value at ca. 34 °C and this value was decreased with the increase of resol concentration in the resol/PEO-*b*-PCL mixtures. More interestingly, this value was further decreased to ca. -43 °C (at 50 wt% resol), -48 °C (at 60 wt% resol), -52 °C (at 70 wt% resol) and disappeared at more than 80 wt% resol concentration. It has been reported that a certain degree of undercooling ($\Delta T = T_m^0 - T_f = 41$ °C, where $T_m^0 = 75$ °C) is required to initiate the crystallization of the PCL segment of the diblock copolymer (e.g., $\Delta T = 50$ °C for lamellar PCL microdomain, and $\Delta T = 125$ °C for cylindrical PCL microdomain).^[28] Therefore, these exotherms should come from the PCL block segment in the 2D cylindrical confinement ($\Delta T = 118\sim 127$ °C).^[11] However, we also observed that the DSC scans display two crystallization exotherms at 50 and 60 wt% resol concentrations, which can be attributed to the fractionated crystallization,^[30-31] where the first crystallization exotherm at a higher value (18~20 °C) is produced by heterogeneous crystallization and the second crystallization exotherm at a lower value (-43~-48 °C) is due to the homogeneous nucleation (independent or non-connecting PCL in 2D cylindrical confinement). **Table 1** summarizes the thermal properties from the heating and cooling scans of resol/PEO-*b*-PCL mixtures based

on DSC analyses, indicating that the blend systems become miscible (single T_g value) at higher resol concentrations since the hydroxyl group of resol could both form the intermolecular hydrogen bonding interaction with the ether group of PEO and the carbonyl group of PCL. In addition, the hydrogen bonding strength or inter-association equilibrium constant (K_A) of the resol/PEO blend ($K_A = 264$) is larger than that of the resol/PCL blend ($K_A = 116$).^[14, 32]

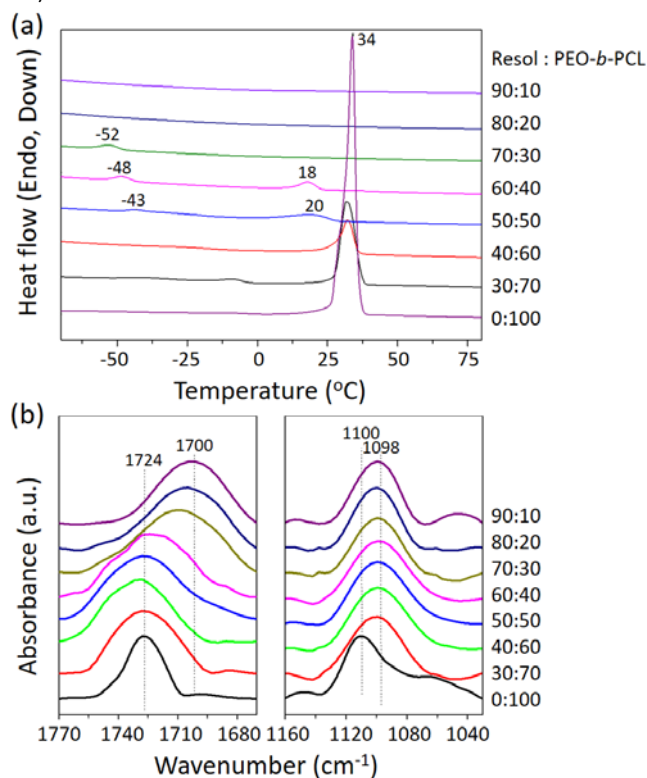


Figure 1. (a) DSC cooling scans of resol/PEO-*b*-PCL mixtures with various resol concentrations. (b-c) FTIR spectra of resol/PEO-*b*-PCL mixtures with various resol concentrations, showing (b) C=O region and (c) ether stretching region.

Table 1. Thermal properties of various resol/PEO-*b*-PCL mixtures

Resol/PEO- <i>b</i> -PCL	T_g (°C)	T_m (°C)	T_c (°C)
0/100	-60	---	65
30/70	-57	-23	64
40/60	-55	-13	58
50/50	-26	-10	55
60/40	-20	-9	51
70/30	-16	2	50
80/20	-12	9	50
90/10	37	---	---
100/0	64	---	---

FT-IR analysis was further carried out to investigate the hydrogen bonding interaction in the resol/PEO-*b*-PCL blend system as shown in **Figure 1b-c**. The FT-IR spectrum of the pure PEO-*b*-PCL diblock copolymer shows the presence of free carbonyl group at 1724 cm⁻¹. In contrast, the FT-IR peak of the H-bonded carbonyl group of PCL at 1700 cm⁻¹ was observed when the resol concentration was at 50 wt% or larger, indicating that the hydroxyl group of resol starts to interact with carbonyl group of PCL as shown in **Figure 1b**. The fraction of the H-bonded carbonyl group of PCL could be resolved by the Gaussian function as mentioned in a previous report.²⁸ In addition, the ether group of the PEO segment (1160~1030 cm⁻¹) is also sensitive to the H-bonding interaction as shown in **Figure 1c**. The pure PEO-*b*-PCL

FULL PAPER

WILEY-VCH

diblock copolymer displays a characteristic band at 1110 cm^{-1} , corresponding to the ether (C-O-C) absorption. However, this characteristic band is shifted to 1098 cm^{-1} at 30 wt% or greater resol concentration due to the H-bonding with resol. As a result, we can conclude that the hydroxyl groups of resol only interact with the ether group of PEO at a relatively lower resol concentration ($< 50\text{ wt}\%$) and interact with both the ether group of PEO and the carbonyl group of PCL at a relatively higher concentration ($> 50\text{ wt}\%$).

Mesoporous Phenolic Resin.

Figure 2 shows the SAXS patterns and TEM images of mesoporous phenolic resin templated by PEO-*b*-PCL diblock copolymer with different resol concentration. Only nanostructures were found at a low resol concentration of 30 wt% based on the SAXS pattern (**Figure 2a**) and TEM image (**Figure 2b**). In comparison, highly ordered mesoporous bicontinuous-gyroid phenolic resin was found at 40 wt% resol concentration based on the SAXS pattern and TEM image (**Figure 2c**). The characteristic $\sqrt{6}:\sqrt{8}:\sqrt{14}:\sqrt{16}:\sqrt{20}:\sqrt{22}$ ratios observed in **Figure S1a** confirm the highly ordered gyroid structure of the obtained mesoporous phenolic resin. The first maximum peak appeared at $\sqrt{6}q^* = 0.21\text{ nm}^{-1}$ ($d = 29.9\text{ nm}$), which $\sqrt{6}q^*$ reflected view from [211] plane, and the cell parameter ' a ' could be determined from the equation of $a = 6^{1/2} d_{211}$ to be 73.2 nm . The detailed characterization results of this highly ordered mesoporous gyroid phenolic resin, including the TEM images viewed from different directions and N_2 adsorption-desorption isotherm are given in **Figure S1a-b**. Furthermore, TEM images of the mesoporous gyroid phenolic resin viewed from different directions are also consistent with the highly order of bicontinuous-gyroid mesoporous structure with $Ia-3d$ symmetry. **Figure S1b** displays the N_2 adsorption-desorption isotherms of the mesoporous bicontinuous-gyroid phenolic resin measured at 77 K , exhibiting the representative type-IV isotherm with a hysteresis loop. In addition, a sharp capillary condensation step was observed at a relative pressure range of 0.45 to 0.85, indicating the uniformity of the mesopores. The mean pore size determined from the adsorption branch was $ca. 12.4\text{ nm}$. The surface area was measured to be $547\text{ m}^2\text{ g}^{-1}$ by the BET method. Further increasing the resol concentration to 50, 60, and 70 wt%, the hexagonal packing cylindrical structure was formed as identified through SAXS analyses (**Figure 2a**), by the definitive $1:\sqrt{3}:\sqrt{4}:\sqrt{7}:\sqrt{9}$ ratio of their scattering peaks, which are consistent with TEM images (**Figures 2d-f**). The TEM images viewed from different directions and N_2 adsorption-desorption isotherms of this highly ordered cylindrical mesoporous phenolic resin (50 wt% resol) are presented in **Figure S1c-d**. It is evident from these

results that the mesoporous phenolic resin obtained at a resol concentration of 50% exhibited apparent reflections with $1:\sqrt{3}:\sqrt{4}:\sqrt{7}:\sqrt{9}:\sqrt{12}:\sqrt{13}:\sqrt{16}$ reflection ratios, revealing the highly ordered hexagonal cylindrical structure. The first maximum peak appeared at $q^* = 0.21\text{ nm}^{-1}$, which corresponded well to the d -spacing of 29.9 nm , as depicted in **Figure 2a**. Furthermore, the TEM images of the mesoporous cylindrical phenolic resin viewed from different directions of [10] and [01] confirmed the highly ordered cylindrical mesoporous structure. **Figure S1d** displays the N_2 adsorption/desorption isotherms of the cylindrical mesoporous phenolic resin, showing the type-IV isotherm with a hysteresis loop. The mean pore size of the cylindrical mesoporous phenolic resin was determined from the adsorption branch to be $ca. 12.2\text{ nm}$. The surface area was measured to be $425\text{ m}^2\text{ g}^{-1}$ by the BET method.

When the resol concentration in the resol/PCL mixtures was increased further to 80 wt%, a disordered structure was found based on SAXS analyses (**Figure 2a**). The broad peak with $1:\sqrt{3}$ reflection ratio corresponds well to a disordered micelle structure, as also confirmed by the TEM image in **Figure 2g**. No obvious peak was found in the SAXS pattern at 90 wt% resol concentration, suggesting the absence of formation of any nanostructures (The TEM image is similar with **Figure 2b**).

Figure 3 summarizes the fraction of H-bonded carbonyl group of PCL (based on the curve fitting results from **Figure 1b**) and pore sizes of different structured mesoporous phenolic resin samples obtained by changing the resol concentration. Clearly, the pore size was decreased with the increase in resol concentration. We know that the hydrogen bonding strength of the resol/PEO blend is stronger than that of the resol/PCL blend, implying that the PEO block segment prefers to interact with the resol, thus acting as the corona domain. However, the weaker H-bonded PCL segment would act as the core domain to induce porosity after calcination, at lower resol concentrations. The fraction of H-bonded carbonyl group was increased with the increase of resol concentration in resol/PEO-*b*-PCL mixtures, as shown in **Figure 3**, implying that the size of the core domain from the PCL segment would decrease and thus, the pore size was decreased with the increase of resol concentration following calcination.

In addition, the morphological transitions of the mesoporous structures from disordered to gyroid to cylindrical and finally to disordered micelle structure were observed with increasing resol concentrations. At higher resol concentrations ($> 80\text{ wt}\%$), a completely miscible, disordered miscible or micelle structure was observed since most of the hydroxyl groups in resol can form H-bonding with both PEO and PCL block segments. However, at lower resol concentrations ($< 30\text{ wt}\%$), the blend

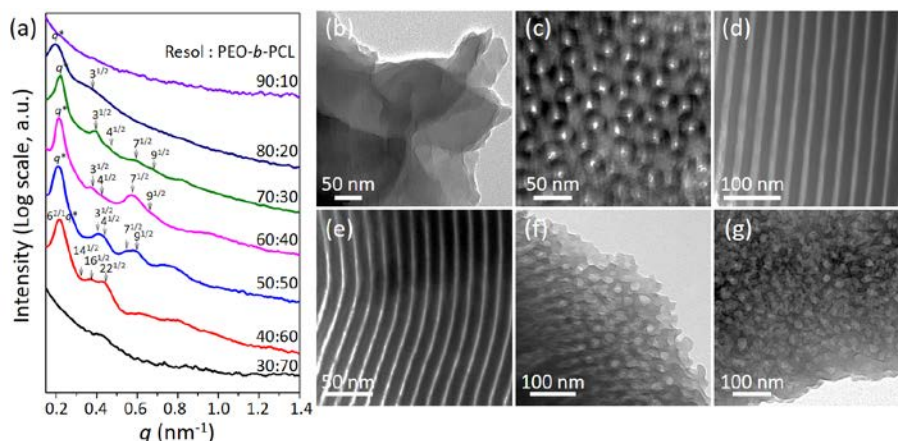


Figure 2. (a) SAXS patterns of mesoporous phenolic resins obtained with various resol concentrations and (b-g) their corresponding TEM images from resol/PEO-*b*-PCL mixtures of (b) 30/70, (c) 40/60, (d) 50/50, (e) 60/40, (f) 70/30, and (g) 80/20

FULL PAPER

WILEY-VCH

system did not have sufficient resol to form the template block copolymer, which exhibited a disordered structure. Therefore, the highly ordered mesoporous phenolic resin was observed only at resol concentrations between 40–70 wt% through the intriguing balance of H-bonding formation and resol concentration.

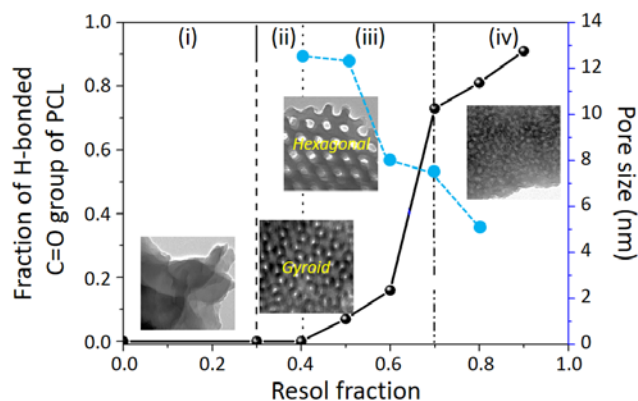


Figure 3. Relationship between the fraction of H-bonded C=O group of PCL and the pore sizes in various self-organized mesoporous phenolic resins.

Mesoporous Carbon Materials.

Mesoporous bicontinuous gyroid structure has received much attention due to their potential use in optical and energy applications.^[33–36] We further investigated the mesoporous gyroid carbon pyrolyzed from mesoporous gyroid phenolic resin under N₂ atmosphere using SAXS, TEM and N₂ adsorption-desorption isotherm, as shown in **Figure 4a–b** and **Figure 5a**. The SAXS pattern in **Figure 4a** displays similar characteristic $v_6:v_8:v_{14}:v_{16}:v_{20}:v_{22}$ ratios and the TEM images of mesoporous gyroid carbon viewed from different directions (**Figure 4b**) are consistent with the highly ordered bicontinuous-gyroid mesoporous structure with $1a-3d$ symmetry. All these results indicate that the highly ordered mesoporous gyroid carbon was thermally stable after calcination under N₂ atmosphere. In addition, the first maximum peak was found at $\sqrt{6}q^* = 0.259 \text{ nm}^{-1}$ ($d = 24.2 \text{ nm}$), which reflects a 19.1 % shrinkage of the carbon framework. The mean pore size of the mesoporous gyroid carbon as determined from the adsorption branch was calculated to be *ca.* 18.1 nm (**Figure 5a** and **Table 2**) based on N₂ adsorption/desorption isotherms measured at 77 K.

We further used the melamine compound to prepare N-doped mesoporous gyroid carbon. **Figure 4c** reveals the similar characteristic peak ratio based on SAXS pattern. Moreover, the TEM images of the N-doped mesoporous gyroid carbon viewed from different directions (**Figure 4d**) are still consistent with the highly order bicontinuous-gyroid mesoporous structure. These results suggest that the highly-ordered nature of the mesoporous carbon was perfectly retained after the thermal treatment with melamine compound. Furthermore, the first maximum peak at $\sqrt{6}q^*$ was shifted to 0.280 nm^{-1} ($d = 22.4 \text{ nm}$). The total shrinkage of the carbon framework for N-doped mesoporous gyroid carbon was 25.1 % compared to the original mesoporous gyroid phenolic resin. In addition, the mean pore size of the N-doped mesoporous gyroid carbon was *ca.* 11.8 nm, as shown in **Figure 5b** and **Table 2**.

Figure 6a displays the Raman spectra of the mesoporous gyroid carbon and the N-doped mesoporous gyroid carbon from 1000 to 3000 cm⁻¹. Two strong peaks attributed to the D band at *ca.* 1334 cm⁻¹ corresponding to disordered carbon and the G band at *ca.* 1590 cm⁻¹ corresponding to the in-plane displacement of carbon atoms in the hexagonal carbon sheets.^[37–39] As a result, the I_D/I_G ratio could be used as the reference for understanding the degree

of graphitization. The mesoporous gyroid carbon possesses an I_D/I_G ratio of 1.01, whereas the I_D/I_G ratio of the N-doped mesoporous gyroid carbon is 1.22. The I_D/I_G ratio of the N-doped mesoporous gyroid carbon was higher than pure mesoporous gyroid carbon, suggesting that the addition of melamine within the mesoporous carbon lowered the degree of graphitization.

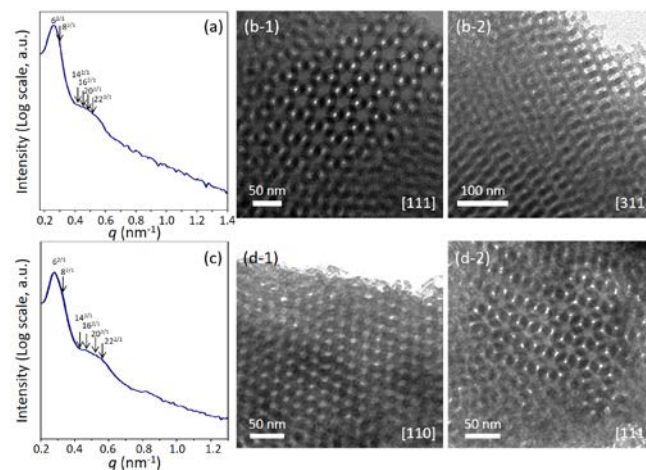


Figure 4. (a) SAXS pattern, and (b) TEM images viewed from [111] and [311] directions planes of mesoporous gyroid carbon. (c) SAXS pattern, and (d) TEM images viewed from [110] and [111] directions planes of N-doped mesoporous gyroid carbon

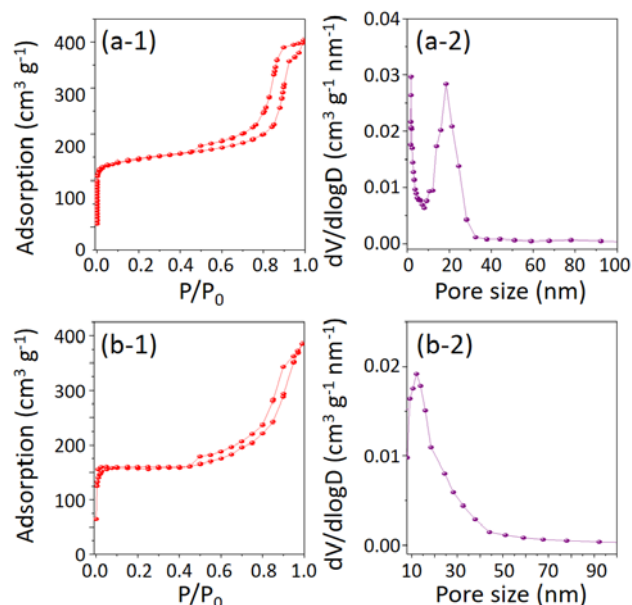


Figure 5. (a-1) N₂ adsorption-desorption isotherm, and (a-2) pore size distribution curve of mesoporous gyroid carbon. (b-1) N₂ adsorption-desorption isotherm, and (b-2) pore size distribution curve of N-doped mesoporous gyroid carbon.

Table 2. Textural properties of mesoporous gyroid phenolic resin, mesoporous gyroid carbon, and N-doped mesoporous gyroid carbon

Samples	Pore Size (nm)	Surface area (m ² /g)	Pore volume (cm ³ /g)
Carbon	18.1	647	0.61
N-doped carbon	11.8	620	0.59

Figure 6b shows the high resolution N1s XPS spectra of the obtained mesoporous N-doped carbon. The nitrogen content is measured to be 2.8 %. Three major types of nitrogen species

could be distinguished on the sample surface: pyridinic-N (398.3 eV, 50.7 %), pyrrolic-N (400.2 eV, 39.0 %), and quaternary-N (401 eV, 10.3%).^[25-27] This result indicates that pyridinic-N and pyrrolic-N are the predominant N species (89.7%) in the obtained mesoporous N-doped carbon. The pyridinic-N has two carbon atoms in the graphitic network, and can form intramolecular H-bonding with the surrounding C-H group. As a result, it can exhibit a stronger Lewis base for enhancing the CO₂ adsorption capacity of the mesoporous carbon.^[26-28] The equilibrium CO₂ isotherms at 0 °C for mesoporous phenolic resin, carbon, and N-doped carbon materials. It can be observed that the CO₂ uptake values of the mesoporous gyroid phenolic resin, mesoporous gyroid carbon and N-doped mesoporous gyroid carbon are 2.36, 4.78 and 6.72 mmol·g⁻¹, respectively (Figure 7). The high CO₂ uptake of the N-doped mesoporous gyroid carbon (6.72 mmol·g⁻¹), is mainly attributed to the high nitrogen content which could effectively promote the adsorption of acidic CO₂ gas, which is also higher than other reported works.^[26-28, 40-46]

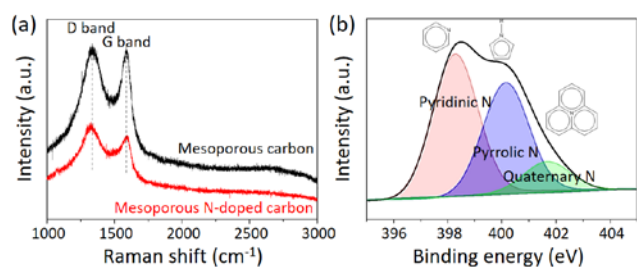


Figure 6 (a) Raman spectra of mesoporous gyroid carbon and N-doped mesoporous gyroid carbon. (b) The high resolution N1s XPS spectrum of N-doped mesoporous gyroid carbon.

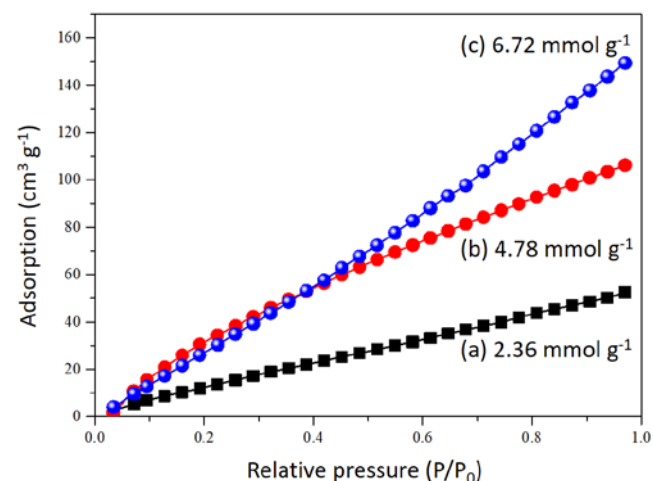


Figure 7 CO₂ capture properties of (a) mesoporous gyroid phenolic resin (b) mesoporous gyroid carbon, and (c) N-doped mesoporous gyroid carbon.

Conclusions

In this work, highly ordered mesoporous phenolic resins with various structures including gyroid and cylindrical structures have been successfully obtained through a soft-templating approach using PEO-*b*-PCL diblock copolymers as templates. Correspondingly, mesoporous carbon with gyroid structure could be obtained from the calcination of the mesoporous gyroid phenolic resins under N₂ atmosphere at 800 °C. The post-treatment of the mesoporous gyroid phenolic resin with melamine resulted in the formation of N-doped mesoporous gyroid carbon with a significantly higher superior CO₂ adsorption capacity (6.72 mmol·g⁻¹), compared to mesoporous gyroid

phenolic resin and undoped mesoporous gyroid carbon. In the future, the adsorption performance of these N-doped mesoporous carbon materials may be further improved by finely tuning the mesostructures, pore sizes, wall thicknesses, and electronic properties through the use of different types of block copolymers and nitrogen sources.

Experimental Section

Materials. The macro-initiator of poly(ethylene glycol) methyl ether with molecular weight of 5,000 was obtained from Sigma-Aldrich and prepared by azeotropic distillation with dry toluene (Acros). The ϵ -caprolactone (ϵ -CL, Acros) monomer was purified using vacuum distillation over calcium hydride (Acros). The catalyst of stannous(II) octoate Sn(Oct)₂ and the solvent of tetrahydrofuran (THF), dichloromethane and *n*-hexane were obtained from Acros. The resol phenolic resin was synthesized from phenol (Acros), formalin (Acros) and sodium hydroxide, NaOH (Acros) through a condensation reaction, and purified using hydrochloric acid (HCl), dichloromethane and magnesium sulfate (MgSO₄, Acros). The N-doped carbonaceous materials were synthesized in dimethyl sulfoxide (DMSO, Acros), in the presence of melamine (Sigma-Aldrich).

Synthesis of PEO-*b*-PCL diblock copolymer. The diblock copolymer was synthesized through ring-opening polymerization (ROP). The monomer ϵ -CL (10 g, 0.088 mol) and the macroinitiator of poly(ethylene glycol) methyl ether (5.0 g, 0.001 mol) and toluene (200 mL) were charged into a flask equipped with condenser and a magnetic stirrer under nitrogen atmosphere. Before refluxing at 150 °C for 18 h, Sn(Oct)₂ (0.8 mg, 0.002 mmol) was added into the flask. Finally, the solvent was removed via rotary evaporation and the white powder was obtained, and then the product of block copolymer was dissolved in dichloromethane and precipitated in the excess of *n*-hexane. The white powder of PEO-*b*-PCL block copolymer was dried in vacuum at 60 °C overnight.

Synthesis of resol-type phenolic resin. The resol-type phenolic resin was obtained from the reaction between phenol and formalin, catalyzed by NaOH solution. Typically, phenol (10.0 g, 106.6 mmol) and 20.0 wt% NaOH solution (2.1 g, 53.5 mmol) were charged into a flask equipped with condenser and were completely melted at 42 °C under stirring. After that, 37.0 wt% formalin (17.2 g, 213 mmol) was added into above mixture under vigorous stirring. The flask was subsequently heated at 70 °C for 1 h and purged with highly pure N₂. Finally, 2.0 M HCl was added dropwise to adjust the pH of the mixture solution to 7.0 and the product was extracted using dichloromethane. After removing the solvent, the liquid product was stored at 0 °C.

Preparation of mesoporous resol-type phenolic resins and carbonaceous materials. Different compositions of resol-type phenolic resin and PEO-*b*-PCL diblock copolymer were dissolved in THF under magnetic stirring. Once the mixture solutions became homogenous, they were placed into aluminum dishes. Next, the THF was slowly evaporated at room temperature and the thermal curing was performed on all of the mixtures by using consecutive heating steps (100 °C for 2 h, 150 °C for 2 h, and 190 °C for 0.5 h). These cross-linked samples were subsequently pyrolyzed by heating them to 330 °C with a slow heating rate of 1 °C·min⁻¹ under inert atmosphere to remove the PEO-*b*-PCL template (a temperature of 330 °C was found to be sufficient for removing the majority of the PEO-*b*-PCL template). The resulting material was identified to be mesoporous phenolic resin. Finally, to obtain the mesoporous carbon, the mesoporous phenolic resin was carbonized in a tubular furnace under highly pure N₂ flow, using a step-wise heating profile (200 °C, 250 °C, 500 °C, and 800 °C with a ramping rate of 5 °C·min⁻¹ and each temperature was maintained

FULL PAPER

WILEY-VCH

for 2 h before increasing the furnace temperature further). To synthesize the N-doped mesoporous carbon, melamine was added into the mesoporous phenolic resin as shown in **Scheme 1**. Briefly, mesoporous phenolic resin (10 mg), melamine (1.5 g) and 15 mL DMSO were mixed at 100 °C under vigorous stirring for 10 h. After drying in vacuum oven at 100 °C for 24 h, the melamine/mesoporous phenolic resin samples were carbonized in a horizontal tube furnace under N₂ atmosphere using the same step heating profile as that used for obtaining pure mesoporous carbon.

Characterizations. DSC thermograms were measured by using the TA-Q20 instrument under the N₂ atmosphere at a heating rate of 20 °C·min⁻¹ from 25 °C to 150 °C for 3 mins and then using 5 °C·min⁻¹ cooling rate from 150 °C to -90 °C to observe the confinement effect of PEO-*b*-PCL diblock copolymer segment. FT-IR samples were prepared by the conventional KBr disk method where the sample thickness should be thinner to obey the Beer-Lambert law. The FTIR spectra were obtained by using the Bruker Tensor 27 spectrophotometer. SAXS data were recorded by using the BL17A1 wiggler beam line at the National Synchrotron Radiation Research Center (NSRRC) in Taiwan. The *d*-spacing was determined by using the $d = 2\pi/q$, where *q* is the scattering vector. TEM images were obtained by using the JEOL 3010 microscope, which operated at 200 kV. In addition, the TEM sample was suspended into the ethanol and then supported onto the holey carbon film on the Cu grid. Nitrogen adsorption/desorption isotherms of the mesoporous samples were determined by using the ASAP 2020 analyzer at 77 K. The samples were degassed under vacuum at 200 °C overnight prior to the BET measurements. The surface area, pore size distribution, and pore volume were obtained by using the BET, BJH, and *t*-plot methods, respectively. Raman spectra was collected using the Jobin-Yvon T6400 micro-Raman machine with He-Cd laser as the excitation source (325 nm) at room temperature. X-ray photoelectron spectroscopy (XPS) was measured by using Mg-K α radiation from the double anode at 50 W. The binding energy was calibrated by using C1s at 284.6 eV for the high-resolution spectra.

Acknowledgements

W.C.C. would like to thank 2014 New Partnership Program for the Connection to the Top Labs in the World, supported by the Ministry of Science and Technology, Taiwan, under contracts MOST 103-2911-I-110-513. This study was also supported financially by the Ministry of Science and Technology, Taiwan, under contracts MOST103-2221-E-110-079-MY3 and MOST105-2221-E-110-092-MY3. This work was partly supported by an Australian Research Council (ARC) Future Fellow (FT150100479), and JSPS KAKENHI Grant Number 17H05393 (Coordination Asymmetry). Y.Y and Z.A.A. are grateful to the Deanship of Scientific Research, King Saud University for funding through Vice Deanship of Scientific Research Chairs.

Keywords: Block copolymer; Bicontinuous gyroid structure; Mesoporous carbon; CO₂ capture

- [1] M. W. Schulze, M. A. Hillmyer, *Macromolecules* **2017**, *50*, 997-1007.
- [2] J. Tang, T. Wang, R. R. Salunkhe, S. M. Alshehri, V. Malgras, Y. Yamauchi, *Chem. Eur. J.* **2015**, *21*, 17293-17298.
- [3] H. C. Lee, H. Y. Hsueh, U. S. Jeng, R. M. Ho, *Macromolecules* **2014**, *47*, 3041-3051.
- [4] H. R. Xue, J. Q. Zhao, J. Tang, H. Gong, P. He, H. S. Zhou, Y. Yamauchi, J. P. He, *Chem. Eur. J.* **2016**, *22*, 4915-4922.
- [5] R. Dawson, A. I. Cooper, D. J. Adams, *Prog. Polym. Sci.* **2012**, *37*, 530-563.
- [6] B. Ouyang, Y. Q. Zhang, Y. Wang, Z. Zhang, H. J. Fan, S. J. Rawat, *J. Mater. Chem. A.* **2016**, *4*, 17801-17808.

- [7] C. Fu, D. Yi, C. Deng, X. Wang, W. Zhang, Y. Tang, F. Caruso, Y. Wang, *Chem. Mater.* **2017**, in press. DOI: 10.1021/acs.chemmater.7b01423
- [8] H. Kosonen, J. Ruokolainen, M. Torkkeli, R. Serimaa, P. Nyholm, O. Ikkala, *Macromol. Chem. Phys.*, **2002**, *203*, 388-392.
- [9] S. Valkama, A. Nykanen, H. Kosonen, R. Ramani, F. Tuomisto, P. Engelhardt, G. ten-Brinke, O. Ikkala, J. Ruokolainen, *Adv. Funct. Mater.* **2007**, *17*, 183-190.
- [10] H. Kosonen, S. Valkama, A. Nykanen, M. Toivanen, G. ten-Brinke, J. Ruokolainen, O. Ikkala, *Adv. Mater.* **2006**, *18*, 201-205.
- [11] D. Hu, Z. Xu, K. Zeng, S. Zheng, *Macromolecules* **2010**, *43*, 2960-2969.
- [12] Y. Deng, T. Yu, Y. Wang, Y. Shi, Y. Meng, D. Gu, L. Zhang, Y. Huang, C. Liu, X. Wu, D. Zhao, *J. Am. Chem. Soc.* **2007**, *129*, 1690-1697.
- [13] Y. Dneg, C. Liu, D. Gu, T. Yu, B. Tu, D. Zhao, *J. Mater. Chem.* **2008**, *18*, 91-97.
- [14] J. G. Li, Y. D. Lin, S. W. Kuo, *Macromolecules* **2011**, *44*, 9295-9309.
- [15] Y. S. Lu, B. P. Bastakoti, M. Pramanik, Y. Yamauchi, S. W. Kuo, *Chem. Eur. J.* **2016**, *22*, 1159-1164.
- [16] J. G. Li, W. C. Chu, U. Jeng, S. W. Kuo, *Macromol. Chem. Phys.* **2013**, *214*, 2115-2123.
- [17] C. Liang, S. Dai, *J. Am. Chem. Soc.* **2006**, *128*, 5316-5317.
- [18] Y. Meng, D. Gu, F. Zhang, Y. Shi, L. Cheng, D. Feng, Z. Wu, Z. Chen, Y. Wan, A. Stein, D. Zhao, *Chem. Mater.* **2006**, *18*, 4447-4464.
- [19] J. Zhang, Y. Deng, J. Wei, Z. Sun, D. Gu, H. Bongard, C. Liu, H. Wu, B. Tu, F. Schuth, D. Zhao, *Chem. Mater.* **2009**, *21*, 3996-4005.
- [20] C. C. Liu, W. C. Chu, J. G. Li, S. W. Kuo, *Macromolecules* **2014**, *47*, 6389-6400.
- [21] J. G. Werner, T. N. Hoheisel, U. Wiesner, *ACS Nano* **2014**, *8*, 731-743.
- [22] K. N. Wood, R. O. Hayre, S. Pylypenko, *Energy Environ. Sci.*, **2014**, *7*, 1212-1249.
- [23] L. Estevez, R. Dua, N. Bhandari, A. Ramanujapuram, P. Wang, E. P. Giannelis, *Energy Environ. Sci.* **2013**, *6*, 1785-1790.
- [24] Y. P. Zhai, Y. Q. Dou, D. Y. Zhao, P. F. Fulvio, R. T. Mayes, S. Dai, *Adv. Mater.* **2011**, *23*, 4828-4850.
- [25] J. Tang, J. Liu, C. Li, Y. Li, M. O. Tade, S. Dai, Y. Yamauchi, *Angew. Chem. Int. Ed.* **2015**, *54*, 588-593.
- [26] L. Wan, J. Wang, Y. Sun, C. Feng, K. Li, *RSC Adv.* **2015**, *5*, 5331-5342.
- [27] L. Wan, J. Wang, L. Xie, Y. Sun, K. Li, *ACS Appl. Mater. Interfaces* **2014**, *6*, 15583-15596.
- [28] L. Wan, J. Wang, C. Feng, Y. Sun, K. Li, *Nanoscale*, **2015**, *7*, 6534-6544.
- [29] W. C. Chen, S. W. Kuo, C. H. Lu, U. S. Jeng, F. C. Chang, *Macromolecules* **2009**, *42*, 3580-3590.
- [30] Y. Y. Huang, J. Y. Hsu, H. L. Chen, T. Hashimoto, *Macromolecules* **2007**, *40*, 3700-3707.
- [31] V. Balsamo, F. von Gyldenfeldt, R. Stadler, *Macromolecules* **1999**, *32*, 1226-1232.
- [32] S. W. Kuo, C. L. Lin, F. C. Chang, *Macromolecules* **2002**, *35*, 278-285.
- [33] M. D. Turner, M. Saba, Q. Zhang, B. P. Cumming, G. E. Schroder-Turk, M. Gu, *Nature Photonics* **2013**, *7*, 801-805.
- [34] J. A. Dolan, B. D. Wilts, S. Vignolini, J. J. Baumberg, U. Steiner, T. D. Wilkinson, *Adv. Opt. Mater.* **2015**, *3*, 12-32.
- [35] S. Choudhury, M. Agrawal, P. Formanek, D. Jehnichen, D. Fischer, B. Krause, V. Albrecht, M. Stamm, L. Ionov, *ACS Nano* **2015**, *9*, 6147-6157.
- [36] H. Y. Hsueh, C. T. Yao, R. M. Ho, *Chem. Soc. Rev.* **2015**, *44*, 1974-2018.
- [37] A. Vinu, P. Srinivasu, M. Takahashi, T. Mori, V. V. Balasubramanian, K. Ariga, *Micro. Mesoporous Mater.* **2007**, *100*, 20-26.
- [38] J. G. Li, C. Y. Tsai, S. W. Kuo, *Polymers* **2014**, *6*, 1794-1809.
- [39] T. V. Reshetenko, L. B. Avdeeva, Z. R. Ismagilov, V. V. Pushkarev, S. V. Cherepanova, A. L. Chuvilin, V. Likhoholov, *Carbon* **2003**, *41*, 1605-1615.
- [40] G. P. Hao, D. W. C. Li, A. Qian, A. H. Lu, *Adv. Mater.* **2010**, *22*, 853-857.
- [41] J. Wei, D. Zhou, Z. Sun, Y. Deng, Y. Xia, D. Zhao, *Adv. Funct. Mater.* **2013**, *23*, 2322-2328.
- [42] T. Chen, S. Deng, B. Wang, J. Huang, Y. Wang, G. Yu, *RSC Adv.* **2015**, *5*, 48323-48330.
- [43] N. P. Wickramaratne, J. Xu, M. Wan, L. Zhu, L. Dai, M. Jaroniec, *Chem. Mater.* **2014**, *26*, 2820-2828.

FULL PAPER

WILEY-VCH

-
- [44] F. Bai, Y. Xia, B. Chen, H. Su, Y. Zhu, *Carbon*, **2014**, *79*, 213-226.
[45] M. Sevilla, A. B. Fuertes, *Eng. Environ. Sci.* **2011**, *4*, 1765-1771.
[46] L. Liu, Z. H. Xie, Q. F. Deng, X. X. Hou, Z. Y. Yuan, *J. Mater. Chem. A* **2017**, *5*, 418-425.

Accepted Manuscript

Table of Content

